AIAA 2002-4701

Wind Tunnel Measurements of Shuttle Orbiter Global Heating with Comparison to Flight

Scott A. Berry, N. Ronald Merski, and Robert C. Blanchard

NASA Langley Research Center,
Hampton, VA 23681

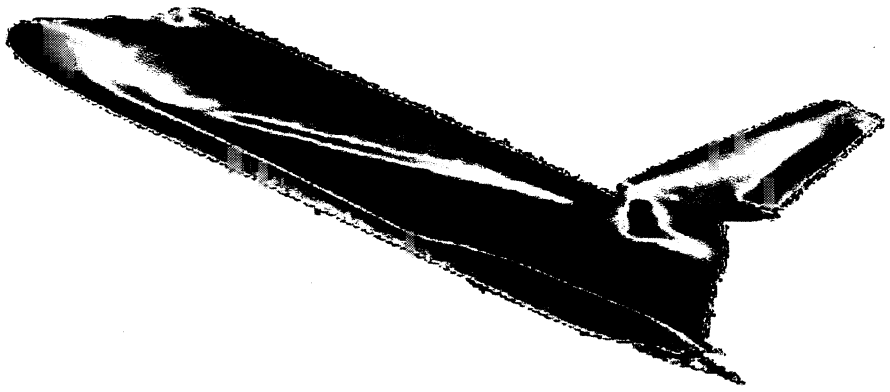

AIAA Atmospheric Flight Mechanics Conference

August 5-8, 2002 / Monterey, CA

For permission to copy or republish, contact the American Institute of Aeronautics and Astronautics
1801 Alexander Bell Drive, Suite 500, Reston, VA 22091

Wind Tunnel Measurement of Shuttle Orbiter Global Heating with Comparisons to Flight

By

Scott A. Berry,*

N. Ronald Merski,†

NASA Langley Research Center, Hampton, VA 23681-2199

and

Robert C. Blanchard‡

George Washington University, JIAFS/NASA-LaRC, Hampton, VA 23681-2199

Abstract

An aerothermodynamic database of global heating images was acquired of the Shuttle Orbiter in the NASA Langley Research Center 20-Inch Mach 6 Air Tunnel. These results were obtained for comparison to the global infrared images of the Orbiter in flight from the infrared sensing aeroheating flight experiment (ISAFE). The most recent ISAFE results from STS-103, consisted of port side images, at hypersonic conditions, of the surface features that result from the strake vortex scrubbing along the side of the vehicle. The wind tunnel results were obtained with the phosphor thermography system, which also provides global information and thus is ideally suited for comparison to the global flight results. The aerothermodynamic database includes both windward and port side heating images of the Orbiter for a range of angles of attack (20 to 40-deg), freestream unit Reynolds number ($1x10^6$/ft to $8x10^6$/ft), body flap deflections (0, 5, and 10-deg), speed brake deflections (0 and 45-deg), as well as with boundary layer trips for forced transition to turbulence heating results. Sample global wind tunnel heat transfer images were extrapolated to flight conditions for comparison to Orbiter flight data. A windward laminar case for an angle of attack of 40-deg was extrapolated to Mach 11.6 flight conditions for comparison to STS-2 flight thermocouple results. A portside wind tunnel image for an angle of attack of 25-deg was extrapolated for Mach 5 flight conditions for comparison to STS-103 global surface temperatures. The comparisons showed excellent qualitative agreement, however the extrapolated wind tunnel results over-predicted the flight surface temperatures on the order of 5% on the windward surface and slightly higher on the portside.

Nomenclature

M	Mach number
Re	unit Reynolds number (1/ft.)
Re_L	length Reynolds number based on L
x	longitudinal distance from the nose (in)
L	model reference length from nose to body-flap hinge line
k	roughness element height (in)
α	model angle of attack (deg)
δ	control surface deflection (deg)
h	heat transfer coefficient (lbm/ft^2-sec) $= q/(H_{aw} - H_w)$ where $H_{aw} = H_{t2}$
h_{F-R}	reference coefficient using Fay-Ridell calculation to stagnation point of a sphere
q	heat transfer rate (BTU/ft^2-sec)
H	enthalpy (BTU/lbm)

Subscripts

∞	freestream static conditions
t1	reservoir conditions
t2	stagnation conditions behind normal shock
aw	adiabatic wall
w	model surface
BF	body flap
SB	speed brake

Introduction

Blanchard, et al. (Ref. 1) discussed the major elements of an experiment called the infrared sensing aeroheating flight experiment (ISAFE). The primary goal of ISAFE is to provide reentry global temperature images from infrared (IR) measurements obtained from a ground-based telescope. These measurements are mainly intended to define the characteristics of hypersonic boundary-layer transition during flight. Specifically, the experiment was initiated to identify, monitor, and quantify hypersonic

* Aerospace Technologist, Aerothermodynamics Branch

† Aerospace Technologist, Aerothermodynamics Branch, Associate Fellow, AIAA

‡ Senior Research Staff Scientist, Associate Fellow, AIAA

boundary-layer windward surface transition of the X-33 vehicle during flight. Global transition images in flight will serve to calibrate and validate current boundary-layer transition prediction techniques; provide benchmark laminar, transitional, and fully turbulent aeroheating data to validate existing experimental and computational results; and advance the state of the art in aerothermodynamic technology.

The initial application of ISAFE was during Shuttle Orbiter flight STS-96 and was used to validate the data acquisition, and data reduction to global temperatures, as reported in Ref. 1. This initial checkout of the system was conducted at the Missile Defense Agency (MDA) Innovative Sciences and Technology Experimentation Facility (ISTEF) site at NASA Kennedy Space Center (KSC) and captured images of the Orbiter during the final approach to the landing site using 24 and 12.5-in. telescopes with mid-wave infrared (MWIR) sensors. During this flight, the Orbiter was tracked for Mach numbers less than two corresponding to the windward surface boundary layer being already turbulent. To acquire Orbiter data at higher Mach numbers before the windward surface begins to transition to turbulence, the IR systems would have to be deployed to sites along the ground track, hundreds of miles away from KSC. To complicate the logistics of planning such a mission, the actual Orbiter ground track can vary significantly from pre-flight nominal due to weather and other considerations that influence the selection of which orbit to begin reentry.

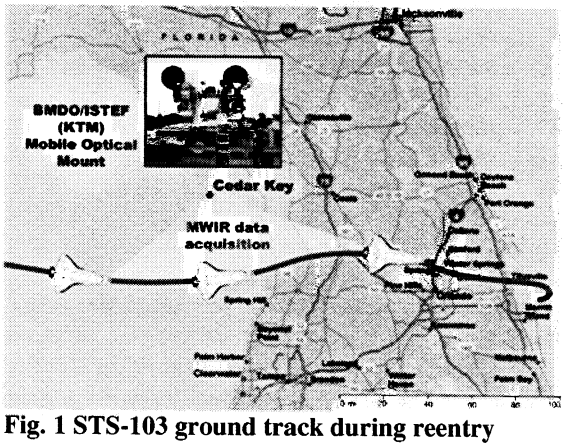

Fig. 1 STS-103 ground track during reentry

A second test of the ISAFE system was conducted on Dec. 27, 1999, during the reentry of STS-103. During this flight, IR images were captured with the MDA/ISTEF equipment deployed to the west coast of Florida. While mobile-mount telescope systems were moved to two locations, Cedar Key and Sanibel Island, only the Cedar Key location successfully captured the shuttle during flight. The ground track of the shuttle, along with the instrumentation located at Cedar Key, is shown in Fig. 1. The IR data was acquired just after shuttle appeared above the horizon, flying at 135,000 ft altitude (with a slant range of about 60.5 miles) and continual images were taken at 30 frames/s as the shuttle flew past and descended down to an altitude of 90,000 ft (with a slant range of roughly 90 miles). This period of acquisition corresponds to Mach numbers between 5.9 to about 3.1. As shown in Fig. 1, the shuttle was conducting a slow turn towards the north as the data was being acquired, which provided a roll of the vehicle such that only the port fuselage was observable during most of the acquisition period. The second site of Sanibel Island (near Clearwater), which was to the south of the ground track, would have been an ideal location to view the windward surface. Unfortunately, the slant angle above the horizon (on the order of 10 deg) was such that the Orbiter never made it above the tree line that was to the north of the Sanibel Island site.

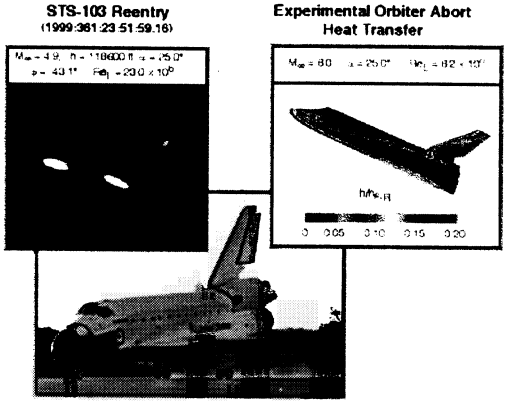

Fig. 2 Initial comparison of STS-103 results to previous wind tunnel measurements

After the STS-103 data was processed, details of which are provided in Ref. 2, the initial comparison to available wind tunnel data showed good qualitative agreement. A typical MWIR image and comparison to previously obtained tunnel results is provided in Fig. 2, along with a post-flight photograph of the shuttle (showing discolorations along the side of the Orbiter that indicate regions of high heating in flight). In the MWIR image, the bright areas of the vehicle qualitatively correspond to regions of higher heating, while the darker regions indicate lower heating. The MWIR image compared surprisingly

well to the wind tunnel results, with bright regions on the nose, along the side of the fuselage, the wing leading edge, and the front of the orbital maneuvering system (OMS) pod. The only region on the flight image that appeared different from the tunnel results is the bright area near the top of the tail. After examination of the post-flight trajectory, it was revealed that the speed brake on the tail was fully deployed at approximately Mach 10. The wind tunnel data acquired prior to the flight did not have the speed brake deployed.

Since the time of the STS-103 flight, new models were built with the speed brake fully deployed and tested in the NASA Langley Research Center (LaRC) 20-Inch Mach 6 Air Tunnel. The wind tunnel data was acquired, on both the Orbiter wind and port sides, utilizing the two-color relative-intensity phosphor thermography system for a wide range of angles of attack, Reynolds number, body flap deflections, speed brake deflections, and with boundary layer trips. Global heating results from the wind tunnel were selected for extrapolation to flight surface temperatures, using the method discussed in Ref. 3. Specifically, a portside global image was extrapolated for comparison to an IR image from the STS-103 flight, while a windward image was selected for extrapolation and comparison to STS-2 discrete thermocouple data. (The windward Orbiter heating images were acquired in anticipation of future ISAFE missions with IR images of the Orbiter windward surface near the time of boundary layer transition.) While the extrapolation method described in Ref. 3 has been successfully compared to predicted flight surface temperatures obtained from computational fluid dynamics (CFD) codes, the present paper, along with the companion paper, Ref. 2, represents the first opportunity to compare to actual flight data. The primary objective of the present paper, therefore, is to provide the details regarding the wind-tunnel database that was acquired for comparison to flight IR images and to discuss some results from the extrapolation method used for predicting flight surface temperatures from wind tunnel global heating images.

Experimental Method

Test Facility

The present experimental results were obtained in the LaRC 20-Inch Mach 6 Air Tunnel. Miller (Ref. 4) provides a detailed description of this hypersonic blowdown facility, which uses heated, dried, and filtered air as the test gas. Typical operating conditions for the tunnel are stagnation pressures ranging from 30 to 500 psia, stagnation temperatures from 760 to 940-degR, and freestream unit Reynolds numbers from 0.5 to 8 million per foot. A two-dimensional, contoured nozzle is used to provide perfect-gas free stream flows with freestream Mach numbers from 5.8 to 6.1. The test section is 20.5 by 20 inches; the nozzle throat is 0.399 by 20.5-inch. A bottom-mounted model injection system can insert models from a sheltered position to the tunnel centerline in less than 0.5-sec. Run times up to 15 minutes are possible with this facility, although for the current heat transfer tests, the model was exposed to the flow for only a few seconds. Flow conditions were determined, based on perfect gas conditions, from the measured reservoir pressure and temperature and the measured pitot pressure at the test section.

Test Technique

The two-color relative-intensity phosphor thermography technique is now routinely being applied to aeroheating tests in the hypersonic wind tunnels of LaRC. Details of the phosphor thermography technique are provided in Refs. 3, 5, and 6. References 7, 8, and 9 are recent examples of the application of this technique to wind tunnel testing. The primary advantage of phosphor thermography is the global resolution of the quantitative heat transfer data. Such data can be used to identify the heating footprint of complex, three-dimensional flow phenomena (e.g., transition fronts, turbulent wedges, boundary layer vortices, etc.) that are extremely difficult to resolve by discrete measurement techniques. Quantitative global surface heating information is obtained from models that can be fabricated quickly (a few weeks) and economically (an order of magnitude less than the thin-film technique). Recent comparisons of heat transfer measurements obtained from phosphor thermography to conventional thin-film resistance gauges measurements (Ref. 10) and CFD predictions (Ref. 11, and 12) have shown excellent agreement.

Model Description

Cast ceramic models of 0.0075 and 0.009-scale Shuttle Orbiter were built in accordance with the procedures detailed in Ref. 13. The models were then coated with a mixture of phosphors suspended in a silica-based colloidal binder. This coating consisted of a 5:1 mixture of lanthanum oxysulfide

(La_2O_2S) doped with trivalent europium and zinc cadmium sulfide (ZnCdS) doped with silver and nickel in a proprietary ratio. The coatings are durable and do not require refurbishment between runs in the wind tunnel, and have been measured to be approximately 0.001 inches thick. The final step in the fabrication process is to apply fiducial marks along the body to assist in determining spatial locations accurately. The fiducial marks used for this investigation were selected to be on the windward surface only and corresponded to the roughness element locations used in Ref. 7 (with the addition of the off-centerline fiducial marks being mirrored on both the port and starboard side of centerline for symmetry). Figure 3 provides a sketch of these windward trip locations (for the 0.0075-scale model), and shows details of the trip dimensions. The Orbiter reference length is based on the body flap hinge line, which for the 0.0075 scale model is located at x=9.7-in and for the 0.009-scale model is 11.6-in.. Three separate models (and back-ups) of the 0.0075-scale Orbiter were built with body flap deflections of 0, 5, and 10-deg (and a speed brake deflection of 0-deg). Figure 4 provides a port side view of the 0.0075-scale Orbiter and identifies the relevant leeside features that will be discussed in the following sections. Two separate models (and back-ups) of the 0.0090-scale Orbiter were built with speed brake deflections of 0 and 45-deg (and a body flap deflection of 0-deg).

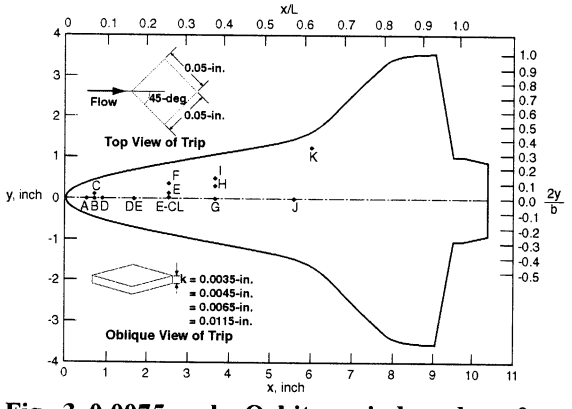

Fig. 3 0.0075-scale Orbiter windward surface showing fiducial mark locations and trips details

The roughness elements used in this study are fabricated to simulate a raised TPS tile and are considered an improvement on the trips used in Ref. 7. During the previous study the trips were cut from 0.0025-inch thick polyimide tape and variations on the roughness heights (k) were obtained by stacking multiple layers of tape (heights of 0.0025, 0.005, 0.0075, and 0.010-inch were used). For the larger trips, there was always the concern that the top layers of the trip could begin to peel up or elastically deform due to the increasing thermal and shear pressure loads present higher in the boundary layer. A new tape, made from polytetraflouroethylene (PTFE) with the same type of adhesive, was obtained which provided nearly the same range in trip height through variations in the PTFE thickness (heights of 0.0035, 0.0045, 0.0065, and 0.0115-inch were available, as shown in Fig. 3). Roughness elements fabricated from PTFE tape were easily applied to the various locations of interest on the model and removed without adversely affecting the phosphor coating.

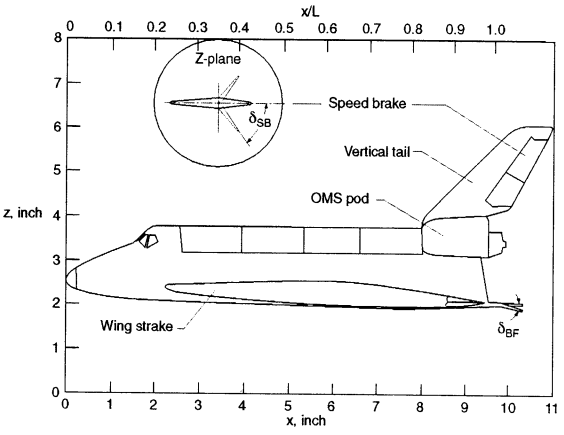

Fig. 4 0.0075-scale Orbiter side details showing body flap and speed brake deflections

Test Conditions

The LaRC 20-Inch Mach 6 Air Tunnel provides a freestream unit Reynolds number (Re) variation of 0.5 to 8.0 million per foot. For the 0.009-scale model where the reference length is nearly one foot, the length Reynolds number (Re_L) is roughly 0.5 to 8.0 million, while for the 0.0075-scale model, the Re_L range is approximately 0.4 to 6.7 million. As discussed in Ref. .14, the Orbiter Re_L in flight at the time of transition can vary from 2.5 to 13 million, which is of the same order of the available wind tunnel range.

Data Reduction

Heating rates were calculated, as discussed in more detail in Refs. 3 and 5, from the global surface temperature measurements using one-dimensional semi-infinite solid heat-conduction equations. Reference 3 provided a discussion on measurement uncertainty, revealing that the phosphor system measurement error was a function

of the surface temperature rise during the run and is typically less than ±10% for windward surface data (but can be significantly higher on the leeside of models where the temperature increase during the run is small). The overall experimental uncertainty of the windward data is approximately ±15%. Heating distributions are presented in terms of the ratio of heat-transfer coefficients h/h_{FR}, where h_{FR} corresponds to the Fay and Ridell[15] stagnation-point heating to a one-foot radius sphere scaled to the model size (a sphere with radius 0.09-in. was used for the 0.0075 scale model, while a 0.108-in sphere was used for the 0.009 scale model). Repeatability of the centerline heat transfer distributions was found to be generally better than ±4%.

Extrapolation Method

The IHEAT data reduction program discussed in Ref. 3 includes an extrapolation method, which provides predicted flight surface temperatures from the global surface phosphor thermography heating data. The use of this method can allow for rapid development of detailed aeroheating information that can be incorporated in the early stages of the vehicle design process. A large experimental database can typically be acquired much quicker and cheaper with the phosphor thermography technique than with a detailed CFD analysis and then extrapolated to the flight trajectory points. The utility and validity of this approach has been shown by recent comparisons of extrapolated wind tunnel data to flight predictions based on CFD for the X-33,[16] X-34,[17] and X-38[9] programs. The present paper represents the first opportunity to compare this method to actual flight results.

A standard approach for extrapolating wind tunnel aeroheating data to flight is to utilize extrapolation factors to adjust the data for differences in Mach number, Reynolds number, or the existence of turbulence, between wind tunnel and flight. Extrapolation factors for both laminar and turbulent flows are developed and discussed in Ref. 3. For laminar flows, the heat transfer coefficient in flight can be estimated based primarily on the velocity difference between flight and wind tunnel to the 0.2 power. For turbulent flows, additional parameters such as the density, wall temperature, and scale differences between wind tunnel and flight must be taken into account. The convective heat transfer rate is then the heat transfer coefficient multiplied by the difference between the adiabatic wall enthalpy and the wall enthalpy in flight. Next, the wall temperature in flight is predicted, based on the assumption that the radiative heat transfer rate away from the surface of the vehicle is equal to the convective heat transfer rate into the vehicle, using the Stefan-Boltzmann law. Thus, the surface temperature in flight to the fourth power is proportional to the heat transfer rate as determined from the extrapolation factor. This simplified relationship is thus the basis for converting the global wind tunnel heating image to predicted surface temperatures at select trajectory points in flight.

Flight Measurements

ISAFE

The objective of ISAFE, a ground-based infrared imagery system, is to monitor the global surface temperatures on the Orbiter in flight for the purpose of capturing the onset of boundary layer transition during the hypersonic portion of the reentry trajectory. Ideally, a global mapping of the movement of transition over the windward surface would serve to calibrate and validate current boundary layer transition prediction techniques. In addition, a goal of the flight experiment is to provide benchmark laminar, transitional, and fully turbulent global aeroheating data for comparison to the discrete flight thermocouple data as well as to ground-based results and computational predictions. To accomplish these goals, long-range ground-based infrared cameras of MDA/ISTEF were utilized to view the Orbiter during STS-103. The ISTEF equipment consists of portable optical tracking mounts, which can be equipped with various telescopes (up to 30-inch apertures) as well as a variety of detectors ranging in wavelength from ultra-violet to the mid-band infrared, which includes the visible. Figure 1 includes an inset showing the mobile tracking mount that was remotely deployed to Cedar Key, FL.

Infrared radiance images are recorded at 30 frames/sec and converted to surface temperatures using the methods described in Ref. 2. The on-board Orbiter surface thermocouples are used as part of the calibration process to convert the infrared data to global temperature images.

Thermocouple Data

The Orbiter on-board data recording system monitors various sensors for post-flight analysis of vehicle performance, including surface thermocouples. The data is recorded at 1-second intervals.

Surface temperatures inferred from the STS-103 flight are used to calibrate the global IR images obtained on the Orbiter port fuselage, as detailed in Ref. 2, for comparison to the extrapolated wind-tunnel images. As windward flight IR images are not yet available, discrete thermocouple data along the centerline from STS-2 will be used for comparison to the extrapolated windward wind-tunnel results.

Discussion of Results

An Orbiter aerothermodynamic database was obtained in the LaRC 20-Inch Mach 6 Air Tunnel for comparison to ISAFE global IR images. The database was acquired in two recent wind-tunnel entries: Test 6815 for windward data and Test 6828 for port side data. Over 70 separate runs in the tunnel were conducted for a range of angles of attack (α of 20, 25, 30, 35, and 40-deg), unit Reynolds numbers (Re between $1x10^6$/ft and $8x10^6$/ft), body-flap deflections (δ_{BF} of 0, 5, and 10-deg), speed-brake deflections (δ_{SB} of 0, and 45-deg), and various boundary layer trips. The wind tunnel results to be shown are representative runs to illustrate the major trends that were observed.

Wind-side Trends

Figure 5 provides the effect of freestream unit Reynolds number on the Orbiter windward heating for α = 40-deg and δ_{BF} = 5-deg. The low Re case shown in Fig. 5a is identical to the lowest Re case (not shown). Also, as shown in Ref. 18, the centerline heating distributions for these low Re cases compare favorably to laminar CFD predictions. Thus, the heating levels over the entire windward surface shown in Fig. 5a are laminar. Note that for the all-laminar case shown in Fig. 5a, a cooler region (identified by violet on the heating scale) is evident in front of the deflected body flap indicating the extent of the separation zone. For the higher Re case (Fig. 5b) the increased heating levels on the body flap, aft fuselage (a little more than halfway along the windward centerline), and wings are indicative of the onset of boundary layer transition. Flow separation in front of the deflected body flap has been removed by the presence of transition ahead of the body flap. Note in Fig. 5b that a slight defect on the model surface has produced a turbulent wedge near the strake leading edge on the lower half of the image.

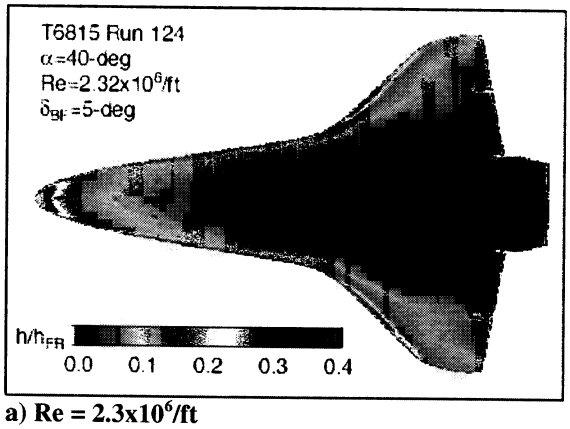

a) Re = $2.3x10^6$/ft

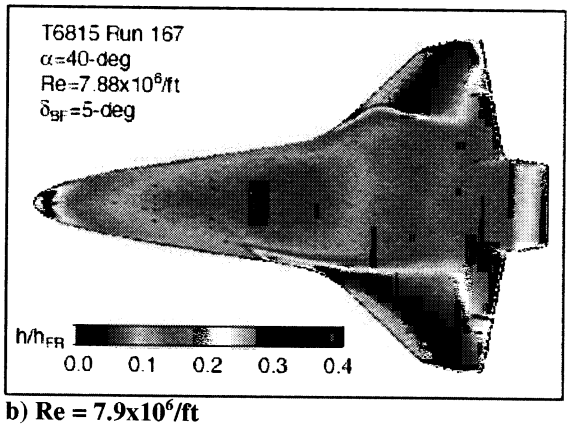

b) Re = $7.9x10^6$/ft

Fig. 5 Effect of Re at α = 40-deg

The effect of angle of attack on Orbiter windward heating at Re = $4.5x10^6$/ft and δ_{BF} = 5-deg is shown in Fig. 6. The heating levels along the windward centerline, which correspond to laminar levels, systematically increase as the angle of attack is increased, as would be expected. The deflected body flap heating levels, however, are increasing more dramatically than the systematic increase on the model centerline, perhaps indicating that transition within the separated shear layer in front of the deflected body flap is being promoted as the angle of attack is increased. The heating levels on the wings are non-laminar for all angles of attack for these moderate Re cases, as a result of the bow shock interaction with the leading edge of the wing, but as the angle of attack is increased, the non-laminar heating levels on the wings increase. Perhaps the effect of the bow shock interaction on the transition process near the leading edge of the wing is increased as the angle of attack is increased.

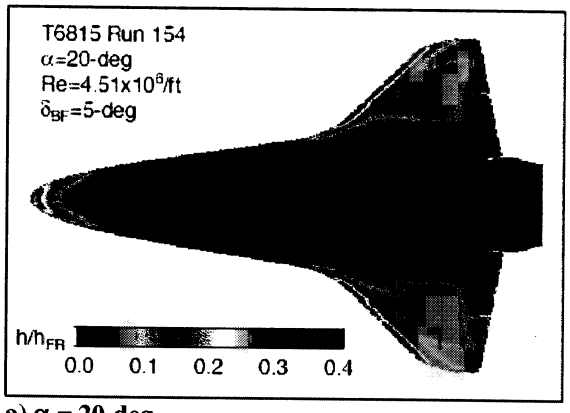

a) α = 20-deg

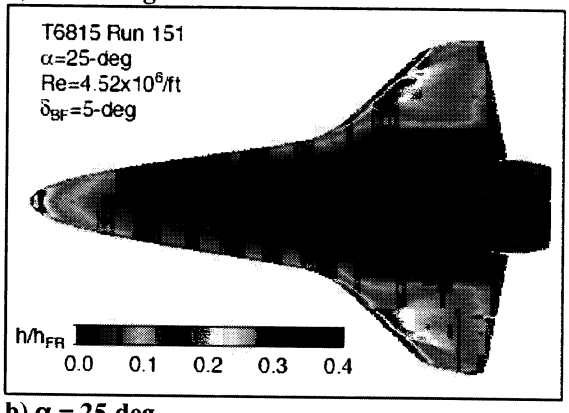

b) α = 25-deg

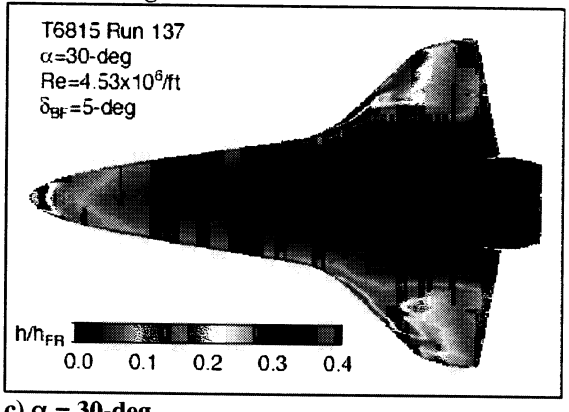

c) α = 30-deg

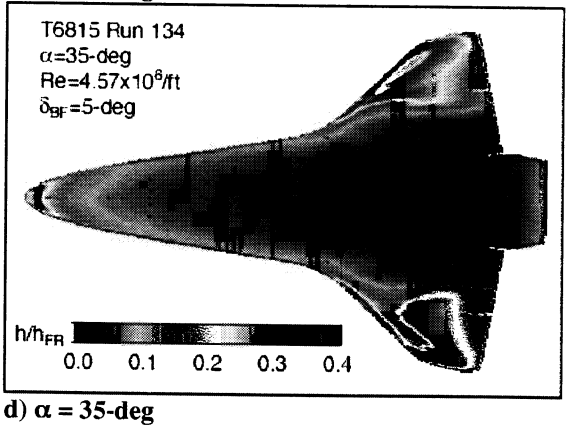

d) α = 35-deg

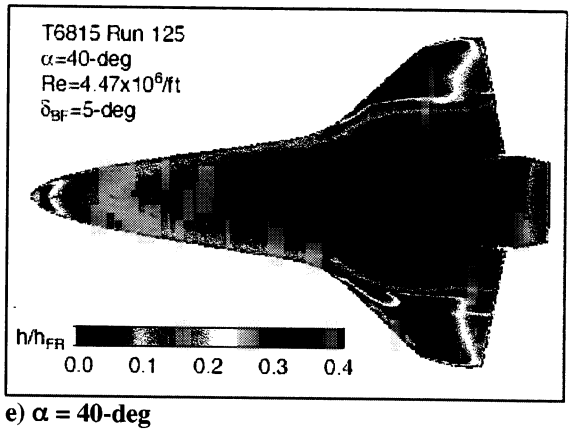

e) α = 40-deg

Fig. 6 Effect of α at Re = 4.5x10⁶/ft

The windward heating images were obtained in anticipation of comparisons to future ISAFE missions with windward flight IR images near the time of boundary layer transition. Therefore, both laminar and turbulent wind tunnel heating levels would allow comparison to the images on either side of the point of transition onset. Wind tunnel results were obtained with forced boundary layer transition using an array of five discrete trips across the model at the x/L = 0.258 station (shown in Fig. 3 as trip locations ECL, E, and F, both port and starboard). The trip heights required to bring transition onset as near to the trip as possible (an effective trip) decreased as the angle of attack increased. The windward forced boundary-layer transition heating images for the angle of attack sweep (same as shown in Fig. 6) for Re = 4.5x10⁶/ft and δ_{BF} = 5-deg is shown in Fig. 7. An interesting note from these images is that the array of fixed trip locations can be useful for qualitatively identifying the location of the attachment lines that run from the stagnation point along the strake towards the wings as a function of angle of attack. For the lowest angle of attack tested, α = 20-deg (Fig. 7a), the turbulent wedges behind each trip is restricted to the windward surface perhaps as an indication that the attachment line is outboard of the outer most trip (location F). By the next angle of attack, α = 25-deg (Fig. 7b), the turbulent wedge is now able to influence the outer edges of the wing, perhaps indicating that the attachment line is in close proximity to the outer most trip. At α = 40-deg (Fig. 7e), the wedges behind the outer most trips are almost swept entirely off the windward surface before the strake even reaches the wing, suggesting that the attachment line is inboard of the F trip location.

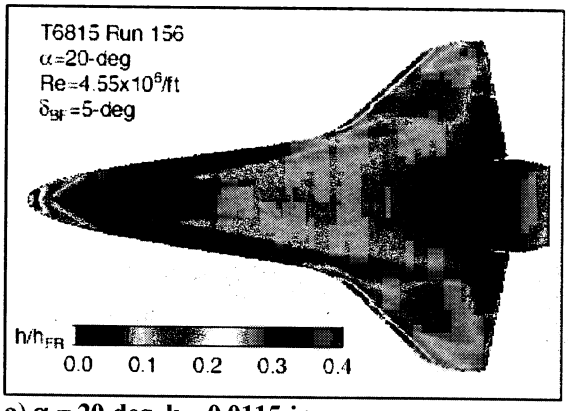

a) α = 20-deg, k = 0.0115-in

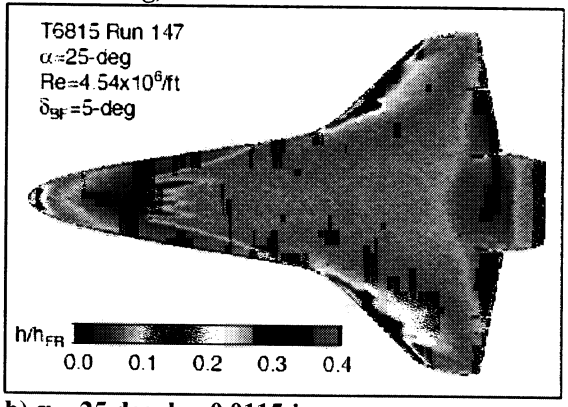

b) α = 25-deg, k = 0.0115-in

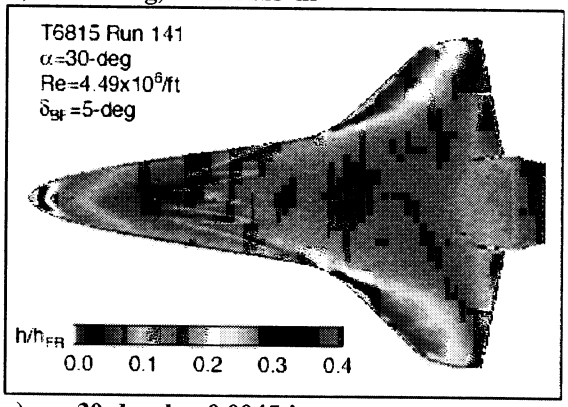

c) α = 30-deg, k = 0.0045-in

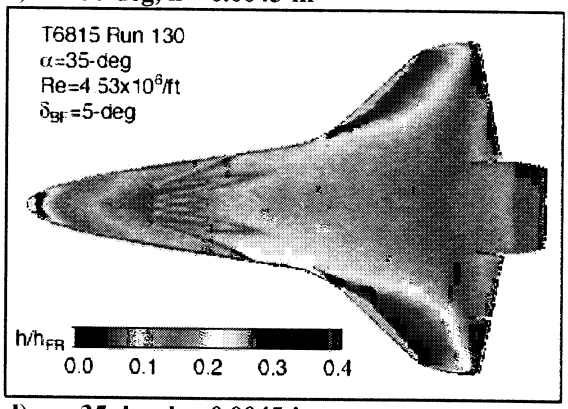

d) α = 35-deg, k = 0.0045-in

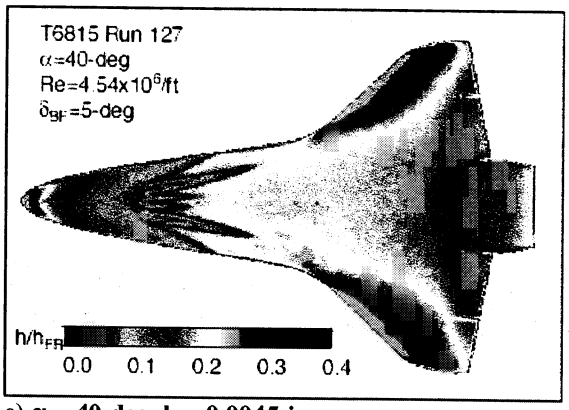

e) α = 40-deg, k = 0.0045-in

Fig. 7 Effect of α with trips at Re = 4.5x10⁶/ft

Lee-side Trends

The effect of freestream unit Reynolds number on the Orbiter port side heating at an angle of attack of 25-deg (corresponding to the reentry angle of attack for STS-103 data) is shown in Fig. 8. These results are for the case with the speed brake fully deployed. Note that the heating scale has been changed from the previous figures. As the unit Reynolds number is increased, the higher heating along the fuselage side from the strake vortex becomes more pronounced and aligns more directly with the OMS pod. Also, the heating on the canopy, the leading edge of the vertical tail, and the deflected speed brake increase as Re increases perhaps as an indication of non-laminar flow. Clearly, based on the Reynolds number effect observed here, as these results are used to extrapolate to even higher flight Reynolds numbers, the location of the vortex streak and subsequent influence on the OMS pod may not be properly accounted for. An interesting note is the evidence of additional small-scale striations within the larger-scale heating streak associated with the strake vortex for the highest Reynolds number case, Re = 7.8x10⁶/ft (Fig. 8b), that had also been observed in Ref. 19 on the Orbiter in both the wind tunnel and flight. There appears to be as many as 5 distinct striations in the image, at an oblique angle to the larger vortex streak that impinges on the OMS pod. In Ref. 19, the striations were attributed to embedded vorticity within the shear layer reattachment of the separated strake flow onto the fuselage, perhaps inducing Goertler-type vortices. As noted in Ref. 19, these striations have been observed in laminar, transitional, and turbulent boundary layers, so their presence here can not be used to infer the boundary layer state.

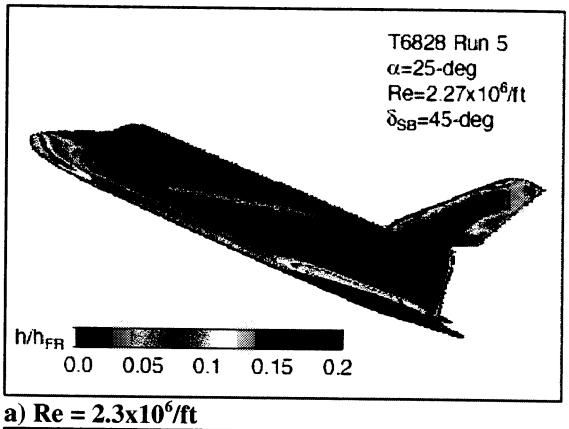

a) Re = 2.3x10^6/ft

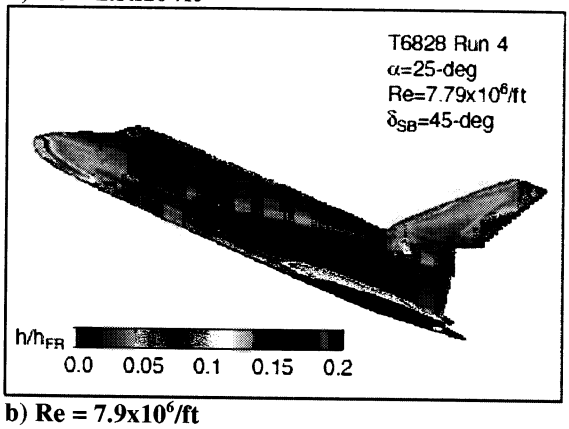

b) Re = 7.9x10^6/ft

Fig. 8 Effect of Re on port heating at α = 25-deg

The effect of angle of attack on the Orbiter port side heating for a freestream unit Reynolds number of Re = 4.5x10^6/ft is shown in Fig. 9. For α = 20-deg (Fig. 9a), the increased heating on the side from the strake vortex is aligned so to impinge directly on the OMS pod. As the angle of attack increases, the vortex scrubbing on the side appears to angle up away from the OMS pod. The heating on the deflected speed brake is higher at the lower angles of attack. The effect of decreasing the angle of attack appears similar to an increase in Reynolds number.

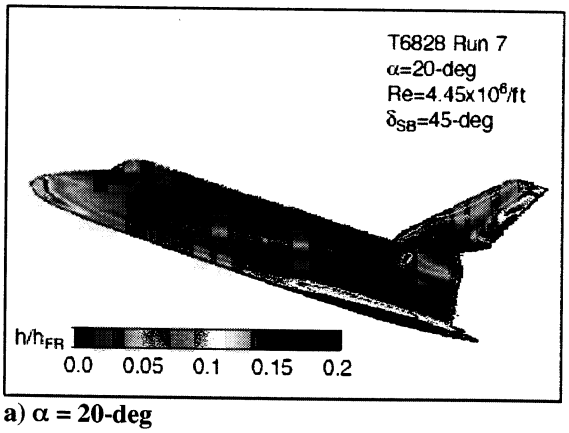

a) α = 20-deg

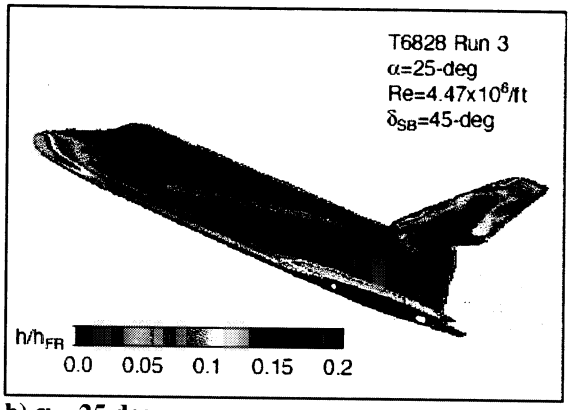

b) α = 25-deg

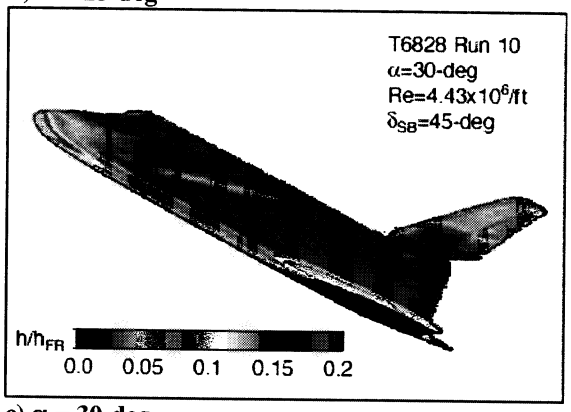

c) α = 30-deg

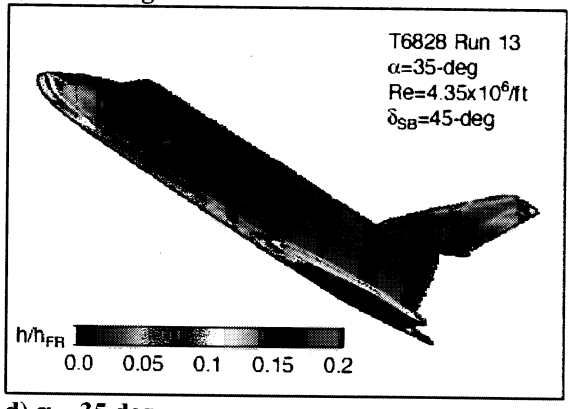

d) α = 35-deg

Fig. 9 Effect of α on port heating at Re=4.5x10^6/ft

Extrapolations to Flight

Unfortunately, ISAFE has yet to obtain a windward global IR image at hypersonic flight conditions. Thus, for the time being, the IHEAT extrapolation method of windward data can only be compared against the flight thermocouple data. As a laminar test case, the flight conditions from STS–2 corresponding to M_∞=11.6 at an altitude of 172-kft. (α=39.6-deg, Re_L = 5.35x10^6, and δ_{BF}=8.3-deg) was selected from the trajectory points reported in Ref. 20. The corresponding laminar wind tunnel case (α=40-deg, Re = 2.2x10^6/ft, and

δ_{BF}=10-deg) was extrapolated to the flight conditions, as shown in Fig. 10. The centerline extrapolated surface temperatures are compared to surface temperatures for the STS-2 flight, as inferred from the thermocouples, in Fig. 11. The temperature levels between the two agree to within roughly 5% with the predictions being higher, except for the body flap region where the flight temperatures are higher despite being at a lower deflection angle than the wind tunnel case (8 in flight vs. 10 in the tunnel). As noted in Ref. 21, the body flap has transitioned to turbulent flow much higher in the flight, nearer to a Mach number of 20. While the flight temperatures on the body flap are likely due to turbulent flow, the wind tunnel results are only transitional and have been extrapolated using laminar factors.

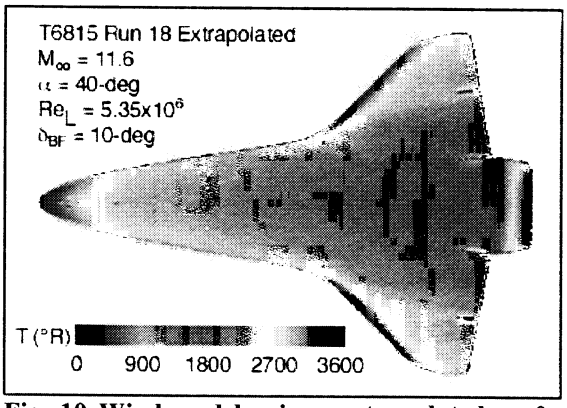

Fig. 10 Windward laminar extrapolated surface temperatures for STS-2 Mach 11.6 case

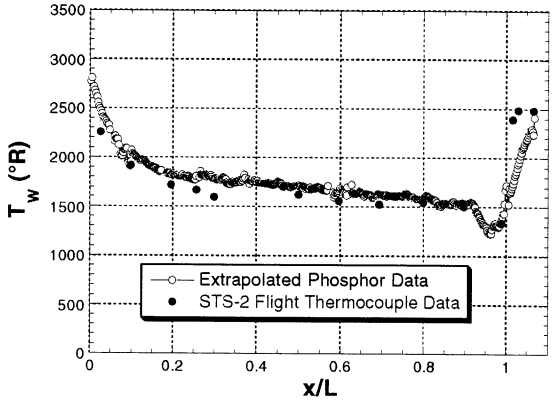

Fig. 11 Comparison of extrapolated results to STS-2 centerline thermocouple data at Mach 11.6

The portside wind tunnel image of the Orbiter model for an angle of attack of 25-deg, freestream unit Reynolds number of 7.8x10^6/ft, with the speed brake fully deployed (δ_{SB}=45-deg) was selected for extrapolation and comparison to a representative STS-103 image. The flight IR temperature mapping corresponds to a M_∞=5.03, altitude of 120.2-kft, length Reynolds number of 21.7 million and an angle of attack of 24-deg. The Orbiter windward surface is turbulent for this low Mach number; therefore, a turbulent extrapolation factor (as detailed in Ref. 3) was used for this leeside case. It should be noted that the extrapolation method was developed for windward attached flows and not for a complex, highly separated leeside flowfield. Nevertheless, the results show good qualitative agreement between the extrapolated wind tunnel data, Fig. 12a, and the flight measurements, Fig. 12b. The vortex scrubbing along the side of the fuselage is clearly evident in both images along with increased surface temperatures at the front of the OMS pod and on the speed brake. In general, the temperatures are on the same order between the extrapolated wind tunnel result and flight with the exception of the red nose and wing in flight, which are saturated beyond the range of the IR camera and the thin vortex streak and tail leading edge, which may not be fully resolved within the pixel resolution of the IR image.

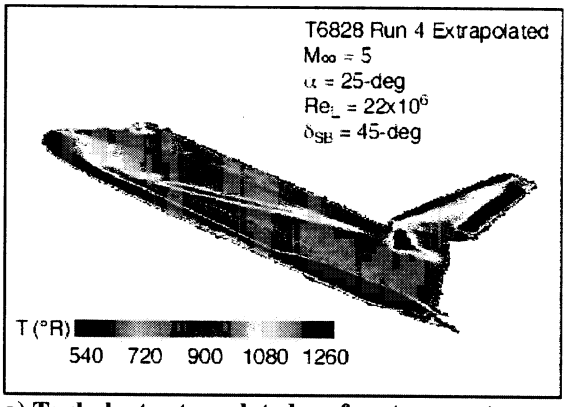

a) Turbulent extrapolated surface temperatures

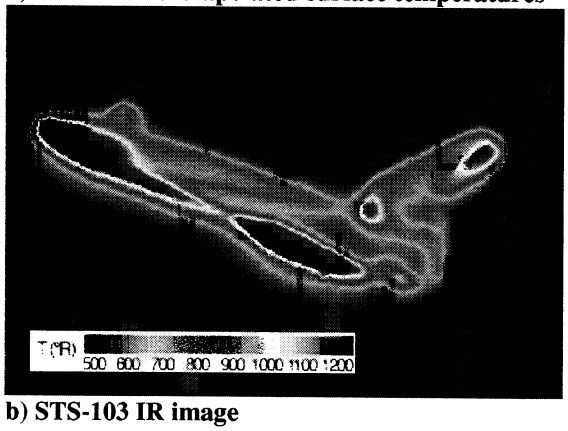

b) STS-103 IR image

Fig. 12 Comparison of portside images between wind tunnel and flight for α = 25-deg

Conclusions

The LaRC 20-Inch Mach 6 Air Tunnel was used to obtain an aerothermodynamic database of global heating images of the Space Shuttle Orbiter. The phosphor thermography technique provided both windward and portside heating images for a range of angles of attack, Reynolds number, body flap deflections, and speed brake deflections. Boundary layer trips were also utilized to obtain non-laminar or turbulent heating levels. These results were obtained to provide inputs to a wind tunnel to flight extrapolation method and thus calibrate/validate this method through comparisons to flight data.

Flight aeroheating data for the Shuttle Orbiter exists in the form of thermocouple measurements and now global temperature images obtained from STS-103 using the Infrared Sensing Aeroheating Flight Experiment (ISAFE). The STS-103 ISAFE results provided port side images, at hypersonic conditions, of the surface temperatures that result from the complex flow features associated with the vortex emanating from the forward portion of the wing strake. Since both the wind tunnel and flight results are global, complex three-dimensional features can be observed and compared. The comparison of the port side wind tunnel results to the STS-103 image for Mach 5 and an angle of attack of 25-deg shows good qualitative agreement. Also, a laminar windward image at an angle of attack of 40-deg was extrapolated to Mach 11.6 flight conditions and compared to STS-2 centerline thermocouple results. Overall, the comparison to the flight windward results was good, with the extrapolated surface temperatures on the centerline being over-predicted by roughly 5% (for a vehicle designer this represents a conservative prediction).

References

1 Blanchard, R. C., Wilmoth, R. C., Glass, C. E., Merski, N. R., Berry, S. A., Bozung, T. J., Tietjen, A., Wendt, J., Dawson, D., "Infrared Sensing Aeroheating Flight Experiment: STS-96 Flight Results," *Journal of Spacecraft and Rockets*, Vol. 38, No. 4, 2001, pp. 465-472.

2 Blanchard, R. C., Anderson, B. P., Welch, S. S., Glass, C. E., Berry, S. A., Merski, N. R., Banks, D. W., Tietjen, A., Lovern, M., "Shuttle Orbiter Fuselage Global Temperature Measurements from Infrared Images at Hypersonic Speeds," AIAA Paper 2002-4702, Aug. 2002.

3 Merski, N. R., "Reduction and Analysis of Phosphor Thermography Data With the IHEAT Software Package," AIAA Paper 98-0712, Jan. 1998.

4 Miller, C. G., "Langley Hypersonic Aerodynamic/ Aerothermodynamic Testing Capabilities - Present and Future," AIAA Paper 90-1376, June 1990.

5 Buck, G. M., "Automated Thermal Mapping Techniques Using Chromatic Image Analysis," NASA TM 101554, April 1989.

6 Buck, G. M., "Surface Temperature/Heat Transfer Measurement Using A Quantitative Phosphor Thermography System," AIAA Paper 91-0064, Jan. 1991.

7 Berry, S. A., Bouslog, S. A., Brauckmann, G. J., and Caram, J. M., "Shuttle Orbiter Experimental Boundary-Layer Transition Results with Isolated Roughness," *Journal of Spacecraft and Rockets*, Vol. 35, No. 3, 1998, pp. 241-248.

8 Berry, S. A., Horvath, T. J., Hollis, B. R., Thompson, R. A., and Hamilton, H. H., "X-33 Hypersonic Boundary Layer Transition," *Journal of Spacecraft and Rockets*, Vol. 38, No. 5, 2001, pp. 646-657 (see also AIAA Paper 99-3560, June 1999).

9 Horvath, T. J., Berry, S. A., Merski, N. R., Fitzgerald, S. M., "X-38 Experimental Aerothermodynamics," AIAA Paper 2000-2685, June 2000.

10 Micol, J. R., "Aerothermodynamic Measurement and Prediction for a Modified Orbiter at Mach 6 and 10 in Air," *Journal of Spacecraft and Rockets*, Vol. 32, No. 5, 1995, pp. 737-748.

11 Hollis, B. R., Horvath, T. J., Berry, S. A., Hamilton, H. H., and Alter S. A., "X-33 Computational Aeroheating Predictions and Comparisons with Experimental Data," *Journal of Spacecraft and Rockets*, Vol. 38, No. 5, 2001, pp. 658-669 (see also AIAA Paper 99-3559, June 1999).

12 Loomis, M. P., Venkatapathy, E., Davies, C. B., Campbell, C. H., Berry, S. A., Horvath, T. J., and Merski, N. R., "Aerothermal CFD Validation and Prediction for the X-38 Program," AIAA Paper 97-2484, June 1997.

13 Buck, G. M. and Vasquez, P., "An Investment Ceramic Slip-Casting Technique for Net-Form, Precision, Detailed Casting of Ceramic Models," U. S. Patent 5,266,252, November 30, 1993.

14 Bouslog, S. A., An, M. Y., and Derry, S. M., "Orbiter Windward Surface Boundary Layer Transition Flight Data," NASA CP-3248, *Orbiter Experiments (OEX) Aerothermodynamics Symposium*, April 1995, pp. 703-739.

15 Fay, J. A., and Ridell, F. R., "Theory of Stagnation Point Heat Transfer in Dissociated Air," *Journal of Aeronautical Sciences*, Vol. 25, No. 2, 1958.

16 Horvath, T. J., Berry, S. A., Hollis, B. R., Liechty, D. S., Hamilton, H. H., and Merski, N. R., "X-33 Experimental Aeroheating at Mach 6 Using Phosphor Thermography," *Journal of Spacecraft and Rockets*, Vol. 38, No. 5, 2001, pp. 634-645 (see also AIAA Paper 99-3558, June 1999).

17 Berry, S. A., Horvath, T. J., DiFulvio, M., Glass, C., Merski, N. R., "X-34 Experimental Aeroheating at Mach 6 and 10," *Journal of Spacecraft and Rockets*, Vol. 36, No. 2, 1999, pp. 171-178.

18 Berry, S. A., and Hamilton, H. H., "Discrete Roughness Effects on Shuttle Orbiter at Mach 6," AIAA Paper 2002-2744, June 2002.

19 Kipp, H. W., and Helms, V. T., "Some Observations on the Occurrence of Striation Heating," AIAA Paper 85-0324, Jan. 1985.

20 Hartung, L. C., and Throckmorton, D. A., "Space Shuttle Entry Heating Data Book Volume I – STS-2," NASA Rept. 1191, Parts 1 and 2, May 1988.

21 Gnoffo, P. A., Weilmuenster, K. J., Alter, S. J., "Multiblock Analysis for Shuttle Orbiter Re-entry Heating from Mach 24 to Mach 12," *Journal of Spacecraft and Rockets*, Vol. 31, No. 3, 1994, pp. 367-377.